ISSN: 2688-8645

Alginate@ Ag_3PO_4 Membranes Prepared with Different Crosslinking Agents and Their Photocatalytic Degradation of Dyes

Xingci Qi[1], Zijia Wang[1], Xiruo Liu[1], Huaidong Wen[1], Haoyu Zhou[2], Shaohan Wei[3], Zelong Gong[1], Kongyin Zhao[1,*], Xiaoyin Wang[2]

[1]State Key Laboratory of Advanced Separation Membrane Materials, Tianjin 300387, PR China

[2]School of Textile Science and Engineering, Tiangong University, Tianjin, 300387, PR China

[3]School of Chemical Engineering and Technology, Tiangong University, Tianjin, 300387, PR China

*tjzhaokongyin@163.com

Abstract

Ag_3PO_4 has attracted attention for its excellent photoresponsive utilization and good catalytic performance. However, Ag_3PO_4 nanoparticles are prone to aggregation and difficult to recycle. In this paper, NaAlg@Ag_3PO_4 photocatalytic material were prepared in-situ growth method using NaAlg as a carrier. And the NaAlg@Ag_3PO_4 water solution was used as the casting solution. Three different crosslinking agents, oxalic acid (OA), $CaCl_2$ and $CuSO_4$, were used to crosslink NaAlg@Ag_3PO_4, resulting in three photocatalytic composite membranes, denoted as OA@NaAlg@Ag_3PO_4, CaAlg@Ag_3PO_4 and CuAlg @Ag_3PO_4. The prepared membranes were tested by infrared spectrum (IR), water contact angle and swelling properties in normal saline. The photocatalytic degradation performance of these membranes for simulated pollutant methyl orange (MO) was studied. The results showed that the composite membrane crosslinked by oxalic acid had good swelling resistance. The photocatalytic degradation performance of OA@NaAlg @Ag_3PO_4 hydrogel membrane was better than that of CaAlg@Ag_3PO_4 and CuAlg@Ag_3PO_4 membranes, and its reusability was the best. Compared with Ag_3PO_4 nanoparticles, the composite hydrogel photocatalytic membrane was easier to operate and recycle.

Keywords

Sodium Alginate; Silver Phosphate; Cross-Linking; Photocatalytic Degradation; Composite Membrane.

1. Introduction

The printing and dyeing industry is developing rapidly, producing a large amount of printing and dyeing wastewater every year. The wastewater contains various organic pollutants, and if discharged directly without treatment, it will cause great harm to the environment[1]. Traditional methods for treating printing and dyeing wastewater include biodegradation[2], physical adsorption[3], and membrane separation[4]. However, these methods have disadvantages such as complex operation, high energy consumption, poor economy, and secondary pollution. Photocatalysis technology has broad prospects in the treatment of industrial wastewater due to its advantages of being green, clean, and cost-effective. Traditional commercial catalysts represented by P25-TiO2 have been widely used in various industries[5]. However, nano semiconductor catalysts face challenges such as difficulty in recycling and

ISSN: 2688-8645

secondary pollution, making them difficult to be widely applied. Therefore, designing a composite catalyst for photocatalytic semiconductor@carrier is particularly important.

Ag_3PO_4, as a visible light responsive catalyst material, has a stronger visible light utilization efficiency than P25-TiO_2, and Ag_3PO_4 has excellent catalytic performance for organic pollutants. Mu Xiao[6] et al. used the molten salt method to prepare atomic Ni cocatalyst on TiO_2 nanoparticles, improving photocatalytic efficiency. Chen[7] et al. encapsulated Ag3PO4 into MIL-101(Fe) to construct Ag_3PO_4/MIL-101 heterojunction composite material, and utilized advanced oxidation techniques such as Fenton catalysis, photocatalysis, and photoFenton catalysis to effectively alleviate the negative impact of tetracycline(TC) on the environment and health. Zhang[8] et al. prepared MoS_2QDs/Ag_3PO_4 composite materials by precipitation method, and studied the photocatalytic performance of Rhodamine B by simulating its degradation under visible light. The degradation rate of Rhodamine B reached 99.6%. Luo[9] et al. prepared Ag_3PO_4 by a simple precipitation method, using crystal violet (CV), methylene blue (MB), and methyl orange (MO) as target pollutants for catalytic degradation under simulated light conditions. The results showed that Ag_3PO_4 had a strong catalytic effect on these three pollutants. Yan Lin[10] et al. successfully prepared a novel photocatalyst Ag_3PO_4@ NC with excellent photocatalytic activity, which can effectively remove organic pollutants. This work provides a universal strategy for constructing built-in electric fields by coupling with NC to improve the catalytic performance of photocatalysts.

In this paper, NaAlg@Ag_3PO_4 photocatalytic material were prepared in-situ and the NaAlg@Ag_3PO_4 water solution was used as the casting solution. Three different crosslinking agents, oxalic acid (OA), $CaCl_2$ and $CuSO_4$, were used to prepare three photocatalytic composite membranes, OA@NaAlg@Ag_3PO_4, CaAlg@Ag_3PO_4 and CuAlg@Ag_3PO_4 membranes. This paper prepared a method for in-situ growth in NaAlg aqueous solution NaAlg@Ag_3PO_4, cast into a membrane. Different photocatalytic composite membranes were obtained by crosslinking NaAlg@Ag_3PO_4 with oxalic acid OA, $CaCl_2$, and $CuSO_4$, respectively. The prepared membrane was characterized and tested. The photocatalytic degradation performance of these membranes for methyl orange was studied.

2. Experimental Section

2.1. Experimental Materials

Sodium alginate (NaAlg) was purchased from Qingdao Mingyue Seaweed Group Co., Ltd. Silver nitrate was purchased from Tianjin Kemio Chemical Reagent Co., Ltd. Sodium phosphate hydrate ($Na_3PO_4 \cdot 12H_2O$) is provided by Tianjin Fengchuan Chemical Reagent Technology Co., Ltd. Sodium carbonate and anhydrous ethanol come from Tianjin Fengchuan Chemical Reagent Technology Co., Ltd; Anhydrous calcium chloride ($CaCl_2$), anhydrous copper sulfate ($CuSO_4$), sodium chloride (NaCl), methyl orange (MO), methylene blue (MB), malachite green (MG), orange yellow G (OG), amaranth red (AR), and rhodamine (RhB) were all purchased from Shanghai Aladdin Biochemical Technology Co., Ltd. All solutions were prepared using deionized water.

2.2. Preparation of NaAlg@Ag_3PO_4

NaAlg@Ag_3PO_4 was prepared by generating Ag_3PO_4 in situ using NaAlg as a carrier. In order to minimize the particle size of Ag_3PO_4 generated, it is necessary to control the droplet acceleration. The preparation steps are as follows: Weigh 1.2 g of NaAlg, dissolve it in 50 ml of deionized water, stir with a magnetic stirrer until a homogeneous solution is formed. Weigh 0.12 g of $AgNO_3$ and dissolve it in 8 ml of deionized water. Calculate $AgNO_3$ at a mass ratio of 10% NaAlg. Add the prepared $AgNO_3$ dropwise to NaAlg, controlling the droplet acceleration so that the $AgNO_3$ is completely dispersed in NaAlg before dropping the next droplet. Dissolve

ISSN: 2688-8645

0.268 g of $Na_3PO_4 \cdot 12H_2O$ in 10 ml of deionized water. Drop the prepared $Na_3PO_4 \cdot 12H_2O$ solution into the NaAlg@$AgNO_3$ solution and control the dripping speed to complete it in half an hour, obtaining an aqueous solution of NaAlg@Ag_3PO_4 as the casting solution.

2.3. Preparation of CaAlg@Ag_3PO_4, CuAlg@Ag_3PO_4 and OA@NaAlg@Ag_3PO_4 membranes

Figure 1 is a schematic diagram of the preparation process of CaAlg@Ag_3PO_4, CuAlg@Ag_3PO_4 and OA@NaAlg@Ag_3PO_4 photocatalytic membranes. Configure the NaAlg@Ag_3PO_4 slowly and evenly pour the casting solution onto a clean glass plate, use a 0.5mm glass rod, and evenly scrape out a liquid membrane with a thickness of 0.5mm. Place the glass plate containing the liquid membrane parallel to an aqueous solution of oxalic acid (OA), $CaCl_2$, and $CuSO_4$ for 12 hours. After the membrane is formed, it can be peeled off from the glass plate for catalytic performance testing.

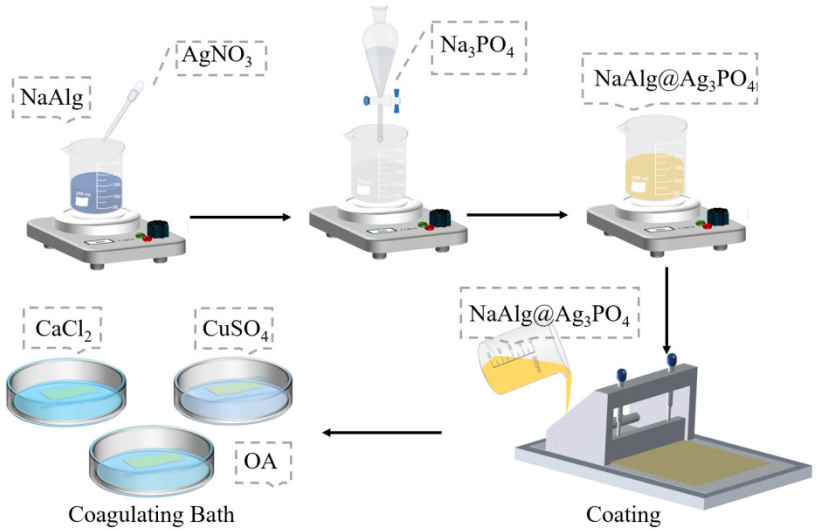

Figure 1. Schematic diagram of photocatalytic membranes preparation process.

2.4. Characterizations

Observe the morphology of Ag_3PO_4 powder under 100 kV conditions using a transmission electron microscope (TEM, Hitachi H7650, Japan). To synthesize NaAlg@Ag_3PO_4,dilute the solution and drop it onto a copper grid using a dropper. After vacuum drying, observe the morphology of the sample using TEM (Hitachi H7650) at 100kV.

The structure of NaAlg, OA@NaAlg, OA@NaAlg@Ag_3PO_4, CaAlg@Ag_3PO_4 and CuAlg@Ag_3PO_4 membranes were tested by Fourier transform infrared spectrometer (Nicolet 6700, Thermo Fisher, America). Perform infrared spectral scanning at a resolution of 2 cm-1, with a scanning wavenumber range of 400-4000 cm-1. Before conducting the test, the sample must be pretreated using a vacuum drying oven (60 ℃, 3h).

The water contact angle of OA@NaAlg@Ag_3PO_4 membrane at room temperature was measured using a dynamic contact angle meter (dsa30s, Kruss, Germany). Fix the membrane on a glass slide using water as the standard liquid. The droplet volume is about 4.5 μ L, and the changes of the liquid on the membrane surface are recorded within 20 seconds. Use Image J software to analyze images and measure contact angles.

2.5. Swelling Performance Test of Hydrogel Membrane

The swelling property of hydrogel membrane was tested by weighing method. The CaAlg@Ag_3PO_4, CuAlg@Ag_3PO_4 and OA@NaAlg@Ag_3PO_4 membranes were made into the same size and weighed (W_0). It was soaked in a 0.9 wt% NaCl solution, taken out at regular intervals,

ISSN: 2688-8645

and weighed. The above experimental operation was repeated to test the swelling rate of the membrane. Generally speaking, the lower the swelling rate, the stronger the membrane's reusability. The swelling rate *Rs (%)* is calculated by equation 1:

$$Rs = \frac{w_t - w_0}{w_0} \times 100\% \quad (1)$$

Wherein, W_0 is the initial mass of the hydrogel membrane (g); Wt is the mass (g) of the hydrogel membrane after swelling in different periods of time. After 2 hours, the swelling of the three membranes reached equilibrium, and the swelling rate after 2 hours was taken as the equilibrium swelling rate.

2.6. Catalytic Degradation Performance Test of Membrane for Dyes

The anionic dye methyl orange (MO) was selected as the target pollutant to test the catalytic performance of photocatalytic membranes prepared with different crosslinking agents. Place three different photocatalytic membranes of the same size in a photocatalytic device for catalytic experiments, take samples at regular intervals, and test the absorbance in a UV spectrophotometer. In the process of photocatalysis, the concentration of dyes can be measured by ultraviolet absorption spectroscopy. According to the Lambert Beer law, the concentration of dye can be determined by measuring the UV absorbance of the solution. The Lambert Beer law formula is as follows:

$$A = K \cdot b \cdot c \quad (2)$$

Among them, K is the molar absorbance coefficient, which is related to the incident light wavelength λ and the properties of the absorbing substance. b is the thickness of the solution absorption layer, which is related to the colorimetric dish. c is the concentration of the absorbing substance. When the testing conditions remain unchanged, the change in dye concentration can be determined based on the UV absorbance. Based on the absorbance value, calculate $1\text{-}C/C_0$ to determine the photocatalytic efficiency.

3. Results and Discussion

3.1. Transmission Electron Microscopy (TEM) Morphology Analysis

Figure 2 shows the transmission electron microscopy (TEM) image of NaAlg@Ag_3PO_4 particles. From Figure 2, it can be seen that Ag_3PO_4 generated in situ using NaAlg as a carrier has a small particle size of approximately 25-50 nm, with an average particle size of 40 nm for Ag_3PO_4. Ag_3PO_4 has good dispersibility in NaAlg, which is related to the in-situ generation of Ag_3PO_4 in NaAlg inhibiting the aggregation of Ag_3PO_4 nanoparticles.

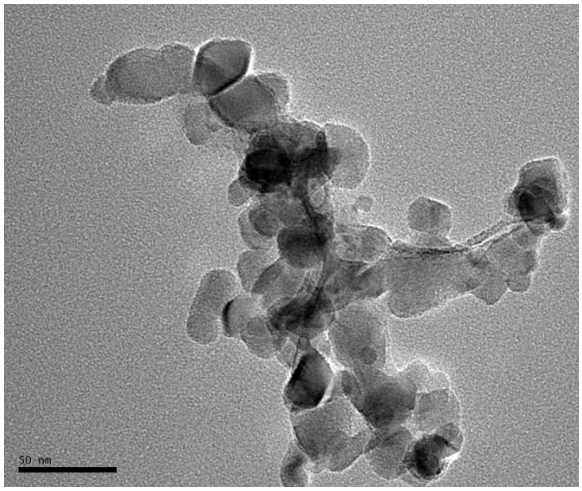

Figure 2. NaAlg@Ag_3PO_4 Transmission electron microscopy image.

ISSN: 2688-8645

3.2. Fourier Transform Infrared Spectroscopy (FT-IR)

Figure 3 shows FT-IR diagram of NaAlg, OA@NaAlg, OA@NaAlg@Ag_3PO_4, CaAlg@Ag_3PO_4 and CuAlg@Ag_3PO_4 hydrogel membranes. The broad peak at 3400 cm^{-1} in the FT-IR spectrum of NaAlg is the vibration of - OH, the peak at 2915 cm^{-1} is the symmetrical vibration of - C-H, the characteristic peak at 1626 cm^{-1} is the anti symmetry of - COOH, the characteristic peak at 1394 cm-1 is the stretching vibration of COO^-, and the characteristic peak at 1027 cm^{-1} is the stretching vibration of C-OH [11]; OA and NaAlg crosslink to form a membrane OA@NaAlg The characteristic peak at 3400 cm^{-1} in the FT-IR spectrum did not show significant changes, but a new characteristic peak appeared at 1707 cm-1, which was a free OA characteristic peak. The characteristic peak at 1626 cm^{-1} showed a shift towards the peak band, due to the interaction between OA and COOH in NaAlg. A new characteristic peak appeared at 1212 cm^{-1}, which was an asymmetric vibration of - OH in OA. The characteristic peak at 1021 cm-1 also shifted towards the peak band compared to the characteristic peak in NaAlg, indicating that C-OH participated in the interaction with OA; Ca^{2+} and NaAlg@Ag_3PO_4 membrane formation CaAlg@Ag_3PO_4 There is a shift towards the peak band at 3400cm^{-1} in the FT-IR spectrum. This indicates that Ca^{2+} has undergone cross-linking with NaAlg [19], and a new characteristic peak appears at 1004 cm^{-1} due to the presence of the P=O bond. 1010 cm^{-1} is the asymmetric stretching peak of PO_4^{3-} [12]. The carboxyl symmetric stretching vibration peak at 1414 cm^{-1} in the spectrum has shifted towards lower wavenumbers, indicating that the functional group is involved in the coordination of Cu^{2+}[13].

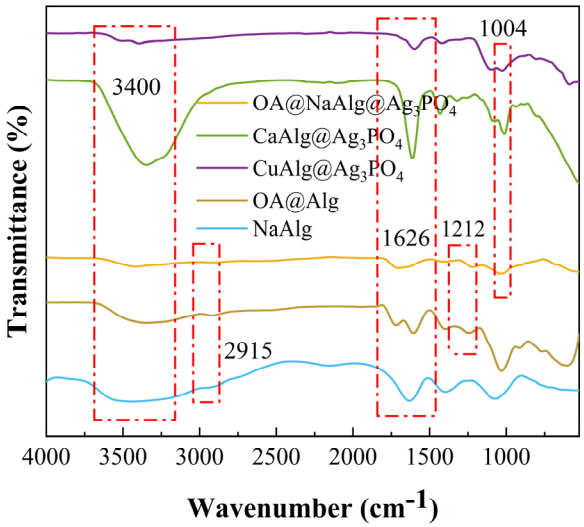

Figure 3. Fourier transform infrared spectrum

3.3. Swelling Performances of Photocatalytic Membranes

Figure 4 shows the swelling rate of CaAlg@Ag_3PO_4, CuAlg@Ag_3PO_4 and OA@NaAlg@Ag_3PO_4 membranes in physiological saline solution. The swelling rates of CaAlg@Ag_3PO_4, CuAlg@Ag_3PO_4 and OA@NaAlg@Ag_3PO_4 hydrogel membrane in 0.9 wt% NaCl solution were 278.3%, 4.6% and 3.4%, respectively. Compared to the CaAlg@Ag_3PO_4 filn, the swelling rate of OA@NaAlg@Ag_3PO_4 membrane decreased by 81.9 times. This is because - COOH selectively binds to divalent metal ions in the D-glucuronic acid (G) segment of β - NaAlg. When there is a large amount of Na^+ in the system, divalent cations will exchange with monovalent cations, thereby reducing the degree of crosslinking [14]. OA can form complex and close electrostatic interactions with NaAlg, increasing cross-linking density [14] [15] [16]. Swelling test instructions OA@NaAlg@Ag_3PO_4 membrane is expected to be used in the treatment of high salt concentration wastewater.

ISSN: 2688-8645

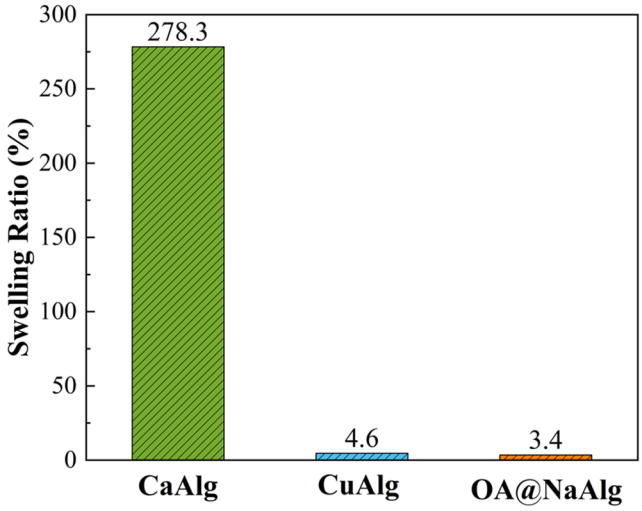

Figure 4. Swelling rate of CaAlg@Ag_3PO_4, CuAlg@Ag_3PO_4 and OA@NaAlg@Ag_3PO_4 membranes in physiological saline solution.

3.4. Contact Angle of Photocatalytic Membranes

Figure 5 shows the static contact angles of CaAlg@Ag_3PO_4, CuAlg@Ag_3PO_4 and OA@NaAlg@Ag_3PO_4 photocatalytic membranes, and the results were 10 °, 12 °, and 16 °, respectively, all of which exhibited good hydrophilicity. The addition of Ag_3PO_4 decreased the contact angle of alginate hydrogel, which was related to the hydrophobicity of Ag_3PO_4.

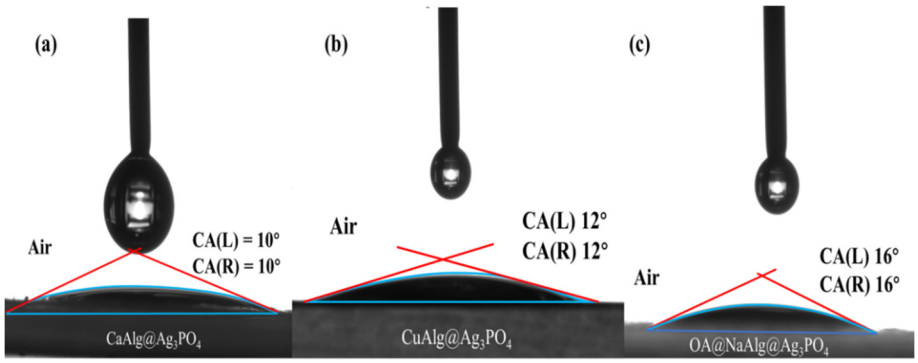

Figure 5. the static contact angles of CaAlg@Ag_3PO_4, CuAlg@Ag_3PO_4 and OA@NaAlg@Ag_3PO_4 photocatalytic membranes.

3.5. Catalytic Degradation Performance of CaAlg@Ag_3PO_4, CuAlg@Ag_3PO_4 and OA@NaAlg@Ag_3PO_4 Membranes Photocatalytic Membrane

Figure 6 shows the degradation effect of MO under three different photocatalytic membranes. From the figure, it can be seen that among the three different crosslinked membranes, OA@NaAlg@Ag_3PO_4 has the best effect and achieves a degradation rate of over 90% for MO. The good catalytic effect of OA@NaAlg@Ag_3PO_4 membrane is attributed to the fact that OA acts as a hole (h+) scavenger, promoting the separation of photo generated electron hole pairs in Ag_3PO_4 [17]. Due to the presence of Ag^+, $C_2O_4^{2-}$ in OA reacts with it to generate AgC_2O_4, which promotes the reaction [18]. Moreover, OA may undergo free radical reactions under light conditions to generate $\cdot OH/\cdot O^{2-}$ [19], promoting the catalytic degradation of dyes. Copper ions may hinder photocatalytic reactions, leading to the poor catalytic effect of the CuAlg@Ag_3PO_4 membrane.

ISSN: 2688-8645

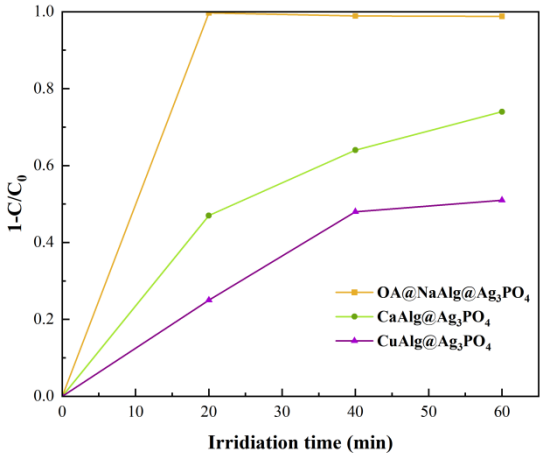

Figure 6. Degradation effect of MO under three different photocatalytic membranes.

3.6. Reusable Performances of OA@NaAlg@Ag_3PO_4 and CaAlg@Ag_3PO_4 Membranes

The stability and recyclability of photocatalysts under illumination are important indicators in practical production. To test its stability and recyclability, a catalyst with better catalytic effect was selected OA@NaAlg@Ag_3PO_4 and CaAlg@Ag_3PO_4 Used for catalytic experiments on MO. The long-term stability of the photocatalytic membrane was obtained by removing the photocatalytic membrane for the next cycle after 60 min of reaction and for three cycles after the second cycle. Figure 7 shows the catalytic effects of CaAlg@Ag_3PO_4 and OA@NaAlg@Ag_3PO_4 photocatalytic membranes on MO at different cycles. It can be seen from the figure that CaAlg@Ag_3PO_4 photocatalytic membrane has poor stability for MO catalysis, and the catalytic effect is only 44% after three cycles. OA@NaAlg@Ag_3PO_4 membrane has the strongest stability, and the catalytic effect on MO is close to 90% after three cycles. The reason for the poor stability of CaAlg@Ag_3PO_4 photocatalytic membrane may be that Ag_3PO_4 is unstable and decomposes into Ag0 when exposed to light, resulting in the decrease of photocatalytic effect.

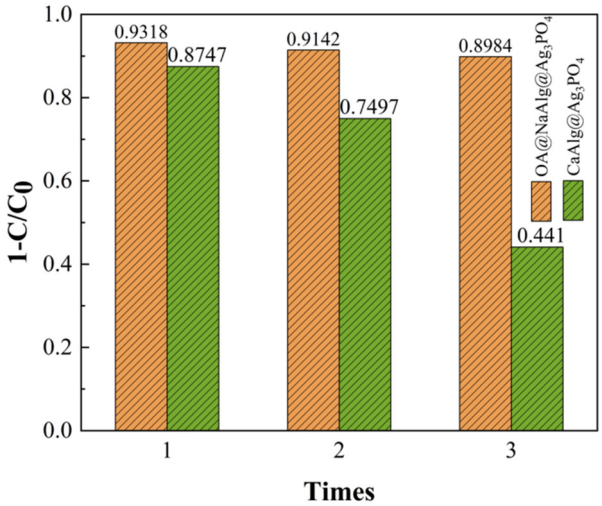

Figure 7. Reusable performance of OA@NaAlg@Ag_3PO_4 and CaAlg@Ag_3PO_4 photocatalytic membranes.

3.7. Study on the Photocatalytic Performance of Different Dye Concentrations

To compare the effects of dye concentration on the performance of different photocatalytic membranes, MO and MB dye solutions were prepared at 5 ppm, 10 ppm, and 20 ppm, respectively. Figure 8 shows the catalytic effect of photocatalytic film on different

ISSN: 2688-8645

concentrations of MO solution. From Figures 8 (a, b, c), OA@NaAlg@Ag_3PO_4 membrane exhibited excellent catalytic performance for MO solutions of different concentrations. The catalytic performance of the CaAlg@Ag_3PO_4 membrane decreased with the increase of MO concentration. The catalytic effect of CuAlg@Ag_3PO_4 photocatalytic film on MO was greatly affected by concentration. From Figure 8 (d, e, f), it can be inferred that the catalytic activity of OA@NaAlg@Ag_3PO_4 towards MB solutions of different concentrations decreased compared to MO solutions, but it still exhibited good photocatalytic performance at lower concentrations, with a catalytic effect of over 95%. The catalytic effect of CaAlg@Ag_3PO_4 was good for lower concentration MB solutions, but poor for higher concentration MB solutions. The catalytic performance of the CuAlg@Ag_3PO_4 membrane towards MB solution decreases with increasing MB concentration.

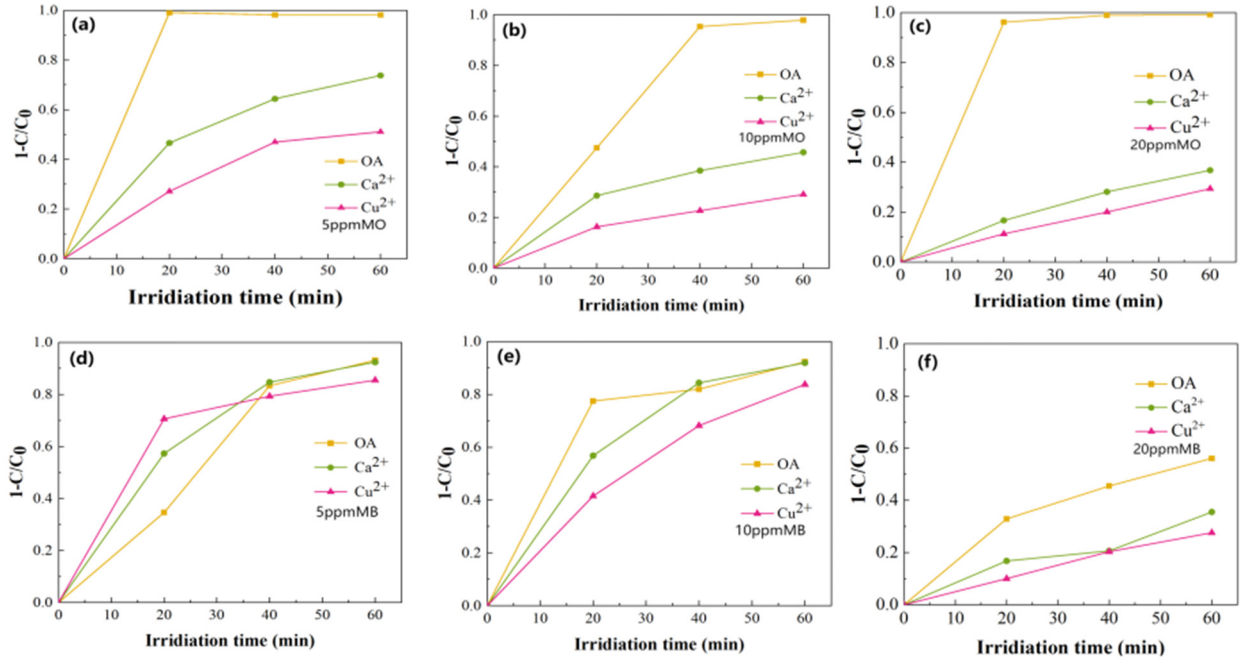

Figure 8. the catalytic effects of different photocatalytic membranes on different concentrations of MO (a, b, c) and MB (d, e, f), (a,d) 5ppm, (b,e)10ppm, (c,f) 20ppm.

4. Conclusion

By using $CaCl_2$, $CuSO_4$, and OA as crosslinking agents, using NaAlg@Ag_3PO_4 as the casting solution, CaAlg@Ag_3PO_4, CuAlg@Ag_3PO_4 and OA@NaAlg@Ag_3PO_4 membranes photocatalytic membranes were prepared. The three membranes were characterized and the photocatalytic catalytic performances of the membranes were investigated. The results show that the hydrophilicity of the three NaAlg@Ag_3PO_4 films decreases compared with that of pure NaAlg, but still maintains good hydrophilicity. OA@NaAlg@Ag_3PO_4 film has excellent anti-swelling properties, which provides feasible evidence for the treatment of salt-containing printing and dyeing wastewater. It has good reusability and has a catalytic degradation performance of nearly 90% for 5 ppm MO after three cycles. In addition, OA@NaAlg@Ag_3PO_4 hydrogels have excellent photocatalytic performance, and the degradation efficiency of the anionic dye methyl orange can reach more than 90%, and it is easy to handle and recover.

Acknowledgments

This work was supported by Tianjin Higher Education Student Innovation and Entrepreneurship Training Program (202410058111).

ISSN: 2688-8645

References

[1] Ewuzie U, Saliu O D, Dulta K, et al. A review on treatment technologies for printing and dyeing wastewater (PDW). Journal of Water Process Engineering, 2022, 50: 103273.

[2] ZHAO S, WANG Z. A loose nano-filtration membrane prepared by coating HPAN UF membrane with modified PEI for dye reuse and desalination. Journal of Membrane Science, 2017, 524: 214-224.

[3] ZHAO H, LIU G, ZHANG M, et al. Bioinspired modification of molybdenum disulfide nanosheets to prepare a loose nanofiltration membrane for wastewater treatment. Journal of Water Process Engineering, 2021, 40: 101759.

[4] TAO X, WANG S, LI Z. Ultrasound-assisted bottom-up synthesis of Ni-graphene hybrid composites and their excellent rhodamine B removal properties. Journal of Environmental Management, 2020, 255: 109834.

[5] Ren H T, Jia S Y, Zou J J, et al. A facile preparation of Ag2O/P25 photocatalyst for selective reduction of nitrate. Applied Catalysis B: Environmental, 2015, 176: 53-61.

[6] ZHANG L, LUO B, et al. Molten-salt-mediated synthesis of an atomic nickel Co-catalyst on TiO2 for improved photocatalytic H_2 evolution. Angewandte Chemie, 2020, 132(18): 7297-7301.

[7] Chen X, Yao L, He J, et al. Enhanced degradation of tetracycline under natural sunlight through the synergistic effect of Ag3PO4/MIL-101 (Fe) photocatalysis and Fenton catalysis: Mechanism, pathway, and toxicity assessment. Journal of Hazardous Materials, 2023, 449: 131024.

[8] Zhang P, Zhao L, Wang Z, et al. Fabrication of MoS2QDs/Ag3PO4 photocatalyst for efficient visible light catalysis. Research on Chemical Intermediates, 2023, 49(11): 5029-5043.

[9] LUO L, LI Y, HOU J, et al. Visible photocatalysis and photostability of Ag_3PO_4 photocatalyst[J/OL]. Applied Surface Science, 2014, 319: 332-338.

[10] LIN Y, YANG C, WU S, et al. Construction of built-in electric field within silver phosphate photocatalyst for enhanced removal of recalcitrant organic pollutants. Advanced Functional Materials, 2020, 30(38): 2002918.

[11] RANA D, MATSUURA T. Surface modifications for antifouling membranes. Chemical reviews, 2010, 110 (4): 2448-2471.

[12] PAHALAGEDARA M N, PAHALAGEDARA L R, KRIZ D, et al. Copper aluminum mixed oxide (CuAl MO) catalyst: A green approach for the one-pot synthesis of imines under solvent-free conditions. Applied Catalysis B: Environmental, 2016, 188: 227-234.

[13] FUKS L, FILIPIUK D, MAJDAN M. Transition metal complexes with alginate biosorbent. Journal of Molecular Structure, 2006, 792: 104-109.

[14] CUI Z Y, SI J, et al. Ionic interactions between sulfuric acid and chitosan membranes. Carbohydrate Polymers, 2008, 73(1): 111-116.

[15] LV X, ZHANG W, LIU Y, et al. Hygroscopicity modulation of hydrogels based on carboxymethyl chitosan/Alginate polyelectrolyte complexes and its application as pH-sensitive delivery system. Carbohydrate Polymers, 2018, 198: 86-93.

[16] ISMAIL O, KIPCAK A S, PISKIN S. Modeling of absorption kinetics of poly(acrylamide) hydrogels crosslinked by EGDMA and PEGDMAs. Research on Chemical Intermediates, 2013, 39(3): 907-919.

[17] DU X, YI X, WANG P, et al. Enhanced photocatalytic Cr (VI) reduction and diclofenac sodium degradation under simulated sunlight irradiation over MIL-100 (Fe)/g-C3N4 heterojunctions. Chinese Journal of Catalysis, 2019, 40(1): 70-79.

[18] Abbasi H, Moradia Z, Ghaedi M, et al. Ag2C2O4/Ag3PO4 composites as efficient photocatalyst for solar light driven.

[19] SERAGHNI N, GHOUL I, LEMMIZE I, et al. Use of oxalic acid as inducer in photocatalytic oxidation of cresol red in aqueous solution under natural and artificial light. Environmental Technology, 2018, 39(22): 2908-2915.